

See discussions, stats, and author profiles for this publication at: <https://www.researchgate.net/publication/235518986>

Enhanced Pseudocapacitance of Ionic Liquid/Cobalt Hydroxide Nanohybrids

ARTICLE *in* ACS NANO · FEBRUARY 2013

Impact Factor: 12.88 · DOI: 10.1021/nn305750s · Source: PubMed

CITATIONS

26

READS

51

10 AUTHORS, INCLUDING:



Bong Gill Choi

Kangwon National University

67 PUBLICATIONS 1,704 CITATIONS

[SEE PROFILE](#)



Minho Yang

National NanoFab Center

28 PUBLICATIONS 821 CITATIONS

[SEE PROFILE](#)



Kyoung G. Lee

National NanoFab Center

43 PUBLICATIONS 334 CITATIONS

[SEE PROFILE](#)



Tae Jung Park

Chung-Ang University

128 PUBLICATIONS 1,563 CITATIONS

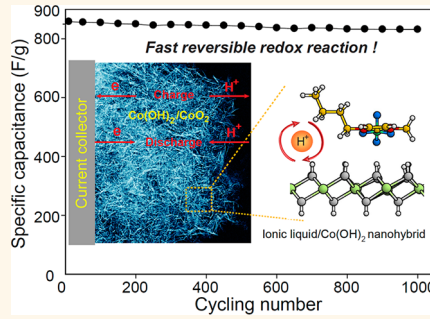
[SEE PROFILE](#)

Enhanced Pseudocapacitance of Ionic Liquid/Cobalt Hydroxide Nanohybrids

Bong Gill Choi,^{†,▽} MinHo Yang,^{†,‡,▽} Sung Chul Jung,[†] Kyoung G. Lee,[#] Jin-Gyu Kim,[§] HoSeok Park,^{||} Tae Jung Park,[¶] Sang Bok Lee,^{‡,⊥} Young-Kyu Han,^{†,×,*} and Yun Suk Huh^{†,□,*}

[†]Division of Materials Science, Korea Basic Science Institute, Daejeon 305-333, Republic of Korea, [‡]Graduate School of Nanoscience and Technology (WCU), Korea Advanced Institute of Science and Technology, Daejeon 305-701, Republic of Korea, [#]Center for Nanobio Integration & Convergence Engineering, National Nanofab Center, Daejeon 305-806, Republic of Korea, [§]Division of Electron Microscopic Research, Korea Basic Science Institute, Daejeon 305-806, Republic of Korea, ^{||}Department of Chemical Engineering, College of Engineering, Kyung Hee University, 1 Seochon-dong, Giheung-gu, Yongin-si, Gyeonggi-do 446-701, Republic of Korea, [¶]Department of Chemistry, Chung-Ang University, 84 Heukseok-ro, Dongjak-gu, Seoul 156-756, Republic of Korea, [⊥]Department of Chemistry and Biochemistry, University of Maryland, College Park, Maryland 20742, United States, [×]Department of Energy and Materials Engineering, Dongguk University-Seoul, Seoul 100-715, Republic of Korea, and [□]Department of Biological Engineering, College of Engineering, Inha University, Incheon 402-751, Republic of Korea. [▽]B.G.C. and M.Y. contributed equally to this work.

ABSTRACT Development of nanostructured materials with enhanced redox reaction capabilities is important for achieving high energy and power densities in energy storage systems. Here, we demonstrate that the nanohybridization of ionic liquids (ILs, 1-butyl-3-methylimidazolium tetrafluoroborate) and cobalt hydroxide (Co(OH)_2) through ionothermal synthesis leads to a rapid and reversible redox reaction. The as-synthesized IL- Co(OH)_2 has a favorable, tailored morphology with a large surface area of $400.4 \text{ m}^2/\text{g}$ and a mesopore size of 4.8 nm . In particular, the IL- Co(OH)_2 -based electrode exhibits improvement in electrochemical characteristics compared with bare Co(OH)_2 , showing a high specific capacitance of 859 F/g at 1 A/g , high-rate capability ($\sim 95\%$ retention at 30 A/g), and excellent cycling performance ($\sim 96\%$ retention over 1000 cycles). AC impedance analysis demonstrates that the introduction of ILs on Co(OH)_2 facilitates ion transport and charge transfer: IL- Co(OH)_2 shows a higher ion diffusion coefficient ($1.06 \times 10^{-11} \text{ cm}^2/\text{s}$) and lower charge transfer resistance (1.53Ω) than those of bare Co(OH)_2 ($2.55 \times 10^{-12} \text{ cm}^2/\text{s}$ and 2.59Ω). Our density functional theory (DFT) calculations reveal that the IL molecules, consisting of anion and cation groups, enable easier hydrogen desorption/adsorption process, that is, a more favorable redox reaction on the Co(OH)_2 surface.



KEYWORDS: supercapacitor · redox reaction · ionic liquid · Co(OH)_2 · nanohybrid

Supercapacitors, which can store electrical energy using faradaic and/or nonfaradaic reactions, are becoming attractive energy storage systems because of their desirable properties, including high power density (10 times higher than batteries), long cyclic lifetime (>100 000 cycles), rapid charging (within seconds), and low maintenance cost.^{1–3} For supercapacitors to truly become an important energy system in the future, however, their energy densities need to be increased.⁴ Although carbon-based electrical double layer capacitors (EDLCs) have already been studied intensively, their charge storage mechanism—which uses the physical adsorption of ions—has limited their specific capacitances. Thus, the development of nanostructured pseudocapacitive materials for supercapacitors is one of the most

important tasks because, in many cases, the energy density arising from redox reactions caused by the adsorption/desorption process of oxidants and reductants at the electrode surface is greater than that of EDLCs.^{5–7} In particular, layered metal hydroxides (e.g., Co(OH)_2 and Ni(OH)_2) have drawn immense attention as alternative capacitive materials to the state-of-the-art amorphous RuO_2 because of their high theoretical capacitance, unique electrochemical properties, low cost, and environmentally benign nature.^{8–11} Most works on such hydroxide-based supercapacitors have concentrated on controlling material geometries to achieve a large surface area, which is related to high specific capacitance; these have included 0D nanoparticles,¹² 1D nanowires,¹³ 2D platelets,^{14–16} and 3D mesoscopic or macroscopic

*Address correspondence to
ykhan@kbsi.re.kr,
yunsuk.huh@inha.ac.kr.

Received for review December 13, 2012
and accepted February 11, 2013.

Published online February 11, 2013
10.1021/nn305750s

© 2013 American Chemical Society

structures.^{17,18} Despite these extensive studies, there is still a significant roadblock when it comes to the implementation of these capacitors, namely, the limited rate charge–discharge capability and continuous cyclability.^{4,19}

The movement of electrons and ions between the inner and outer boundaries of electrode materials is central to the high-performance supercapacitors.^{20–22} In most cases, pseudocapacitors suffer from relatively poor rate capability and durability compared to EDLCs because of the irreversibility of redox reactions originating from the physicochemical changes that take place during charging/discharging. Thus, the rapid and reversible redox reaction of the nanostructured materials accompanying the efficient charge propagation is highly desirable for achieving both high energy and power densities in pseudocapacitors. The rate characteristics of most nanostructured materials face fundamental scientific challenges, mainly in terms of the intrinsic properties associated with slow kinetics, poor electrical conductivity, and weak mechanical stability.²⁰ Apart from the kinetics issue, the surface shield is also essential in maintaining the capacitance during long cycling because side reactions with electrolytes, structure collapse, and reagglomeration into large grains may lead to a high level of irreversibility, all of which are responsible for poor cycle life.²⁰ Accordingly, to achieve high power and energy density of supercapacitors with a long cycle life, comprehensive nanoscale engineering should be incorporated into the fabrication of capacitive materials, taking full account of morphology, pore size and distribution, redox active sites, and mass transport pathways.

Ionothermal synthesis, along with the structure and functional-directing role of ionic liquids (ILs), has been introduced as a novel synthetic route for fabricating inorganic nanomaterials and IL/inorganic hybrids with interesting morphologies and properties.^{23–25} Moreover, ILs in hybrid structures of nano-objects, including polymers, metals, and carbon allotropes, lead to the rendering of new and multifunctionalities to constitutive materials, and thus alter the characteristics of solubility, wettability, chemical reactivity, and charge and energy transfer.^{26–31} Nevertheless, in the application of ILs for energy storage devices, most recent works have concentrated on improving the solvent potential of ILs, including the electrochemical window and ionic conductivity for electrolyte materials.^{32–34} For instance, Moganty *et al.* recently reported that ZrO₂/IL hybrid materials exhibited a wide redox stability window and good thermal and mechanical stability.³⁵ Less attention has been paid to IL-based hybrid electrode materials for energy applications, in particular supercapacitors, even though the aforementioned unique properties of ILs in hybrid structures can significantly improve the high capacitive properties. In addition, a fundamental understanding of electrochemical behavior and charge transfer of ILs

and inorganic hybrid electrodes has yet to be generated.

In this work, we report on the synthesis of imidazolium-IL functionalized-cobalt hydroxide nanohybrids (IL-Co(OH)₂) through a facile ionothermal method. Here, 1-butyl-3-methylimidazolium tetrafluoroborate ([Bmim][BF₄]) was selected as imidazolium-IL because of its unique properties, including high ionic conductivity, hydrophilicity, and a good structural guiding template. The tailored geometric morphology and chemical structure of the IL-Co(OH)₂ hybrid were successfully prepared with a mesopore size of 4.8 nm and Brunauer–Emmett–Teller (BET)³⁶ surface area of 400.4 m²/g through modifying the Co(OH)₂ surface with ILs. In particular, ILs in this hybrid structure played an essential role in facilitating ion diffusion behavior, charge transfer, and hydrogen desorption/adsorption process, thus leading to rapid and efficient redox reaction of Co(OH)₂. This enhancement of redox reaction of the IL-Co(OH)₂ enabled further improvement of the supercapacitive performances, compared with the bare Co(OH)₂, showing a high specific capacitance of 859 F/g at 1 A/g, high rate capability (~95% retention at 30 A/g), and excellent cycling performance (~96% retention over 1000 cycles).

RESULTS AND DISCUSSION

Figure 1 panels a–c show low- and high-resolution transmission electron microscope (TEM) images of IL-Co(OH)₂ nanohybrids after removing the unbounded ILs with intensive washing steps. It could be clearly observed that the porous network structure consists of agglomerated and wrinkled thin Co(OH)₂ nanosheets. In contrast, the bare Co(OH)₂ without the ILs exhibited an irregular size and shape under the same experimental conditions as those of the IL-Co(OH)₂ hybrid (see Supporting Information, Figure S1). This result suggests the functional role of ILs as templates for the preparation and stabilization of Co(OH)₂ nanostructures. When observing individual IL-Co(OH)₂ (Figure 1d), the distance between two adjacent lattice planes (*d* spacing) is approximately 0.236 nm. This length corresponds to the interplanar distance of the Co(OH)₂ (011) plane, as confirmed by the X-ray diffraction (XRD) result (Figure 1e). To determine the phase structure, XRD measurements were taken for IL-Co(OH)₂, bare Co(OH)₂, and [Bmim][BF₄], as shown in Figure 1e. All XRD patterns of both the IL-Co(OH)₂ and Co(OH)₂ products indicate the formation of the hexagonal phase of brucite³⁷-like β-Co(OH)₂ (JCPDS card no. 74-1057 with lattice constants *a* = 3.17 Å and *c* = 4.64 Å).³⁸ Figure 1f shows the N₂ adsorption/desorption isotherms and pore size distribution of the IL-Co(OH)₂ nanohybrids. The hysteresis loop of the type IV isotherm³⁹ indicates the existence of large mesopores, and a narrow pore size distribution of 4.8 nm was observed (inset of Figure 1f). In contrast, Co(OH)₂ showed a different hysteresis

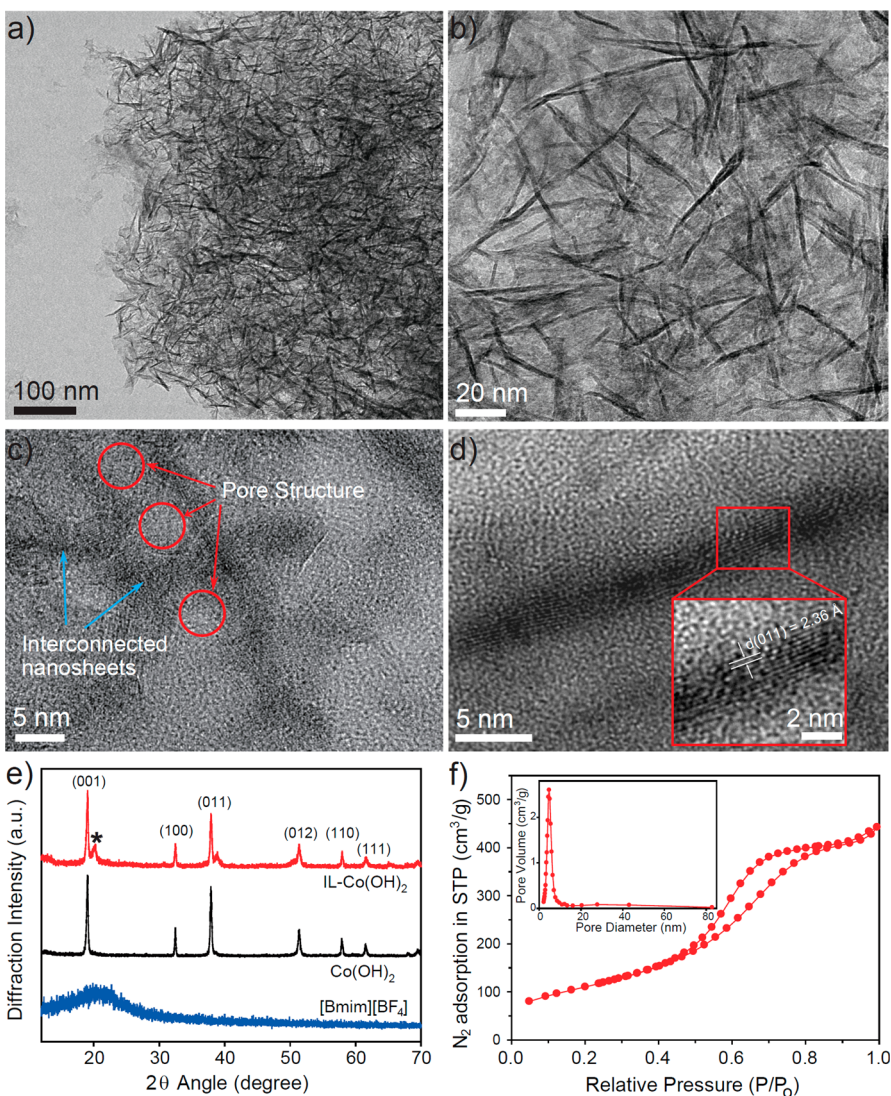


Figure 1. (a–d) TEM images of IL-Co(OH)₂ (inset of image d shows a lattice image of individual IL-Co(OH)₂); (e) XRD patterns of IL-Co(OH)₂, Co(OH)₂, and [Bmim][BF₄]; (f) N₂ adsorption/desorption isotherms and pore size distribution of IL-Co(OH)₂.

curve with broad pore size distribution (Supporting Information, Figure S2). In particular, a surface area of 400.4 m²/g for IL-Co(OH)₂, which was obtained from the BET equation, was about 6-fold higher than 72.3 m²/g for Co(OH)₂ (Supporting Information, Table S1). The large mesopores with narrow pore size distribution of the nanostructured IL-Co(OH)₂ hybrid were attributed to the formation of a nanoporous network as a consequence of agglomeration of wrinkled ultrathin cobalt hydroxide nanosheets. Therefore, the superior textural properties of the nanostructured IL-Co(OH)₂ hybrid are expected to be suitable for an advanced capacitive material, enabling fast ion diffusion and easy accessibility into the mesopore structure.

To investigate the formation mechanism of the nanohybridization of IL-Co(OH)₂, Fourier transform infrared (FT-IR), and X-ray photoelectron spectroscopy (XPS) were applied. Previous reports proposed the hydrogen bond-co- $\pi-\pi$ stacking mechanism for the formation of the self-assembled IL-inorganic

nanomaterials as proved by FT-IR spectroscopy.^{25,40,41} In an IL-assisted synthetic system, the oriented stacking structure of cylindrical micelles of ILs via $\pi-\pi$ interactions⁴² between the imidazolium (cationic salts of ILs) rings offers soft templates for nanostructures. Meanwhile, an effective bridge of nanostructured inorganics and ILs is formed through the hydrogen bonds between them. The self-organization of the [Bmim][BF₄]-Co(OH)₂ hybrids was demonstrated by FT-IR results as shown in Figure 2a. Compared with the bands of pure [Bmim][BF₄], the bands related to the imidazolium ring such as 1059 cm⁻¹ for ν_{C-N} stretch,⁴³ 1169 cm⁻¹ for ν_{skeleton} stretch,⁴⁴ and 3103 cm⁻¹ and 3149 cm⁻¹ for ν_{C-H} stretch,⁴⁰ broadened and shifted in the hybrid structure, indicating the $\pi-\pi$ stack of the imidazolium ring. The bare Co(OH)₂ exhibited two prominent bands at 509 cm⁻¹ for ν_{Co-OH} bending and 3627 cm⁻¹ for ν_{-OH} stretch.³⁸ In contrast, the OH stretching band at 3627 cm⁻¹ was red-shifted and broadened in the IL-Co(OH)₂ hybrid at 3624 cm⁻¹ due to the

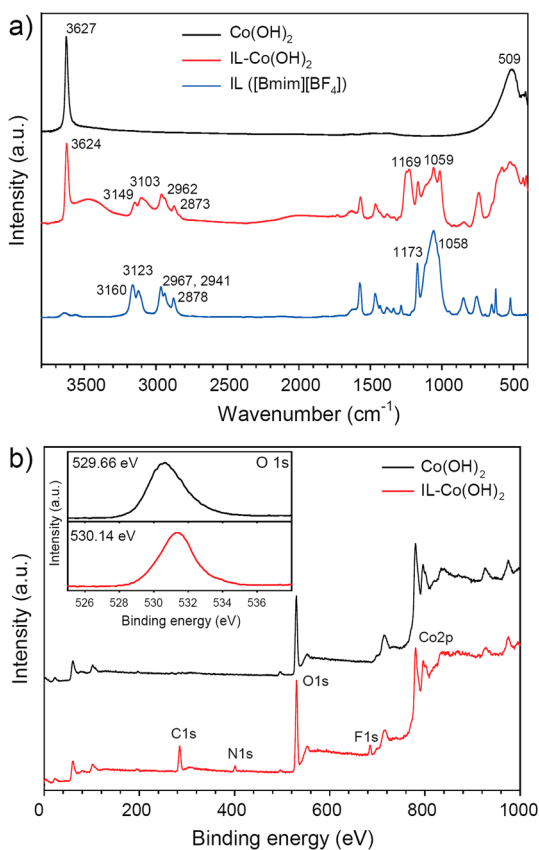


Figure 2. (a) FT-IR spectra of IL-Co(OH)₂, Co(OH)₂, and [Bmim][BF₄]; (b) XPS survey spectra of IL-Co(OH)₂, and Co(OH)₂ (inset is O 1s spectra of IL-Co(OH)₂ and Co(OH)₂).

perturbation of hydrogen bonding between the ([Bmim][BF₄])-BF₄·HO(Co(OH)₂).⁴⁰ Obviously, the formation of π - π stacking of self-assembled ILs was further observed in the XRD patterns (Figure 1e). In comparison with the Co(OH)₂, the IL-Co(OH)₂ hybrid revealed the emergence of an additional peak around 20° (an asterisk mark in Figure 1e) which corresponds to the self-ordering of the imidazolium rings of ILs.²⁵ This result indicates that both the formation and growth of cobalt hydroxide crystallites were induced by mutual interactions between ILs and Co(OH)₂. The characterization of the chemical structure for the IL-Co(OH)₂ hybrid was also confirmed by XPS spectra, as shown in Figure 2b. The newly appearing C 1s, N 1s, and F 1s peaks of the IL-Co(OH)₂ hybrid, compared with the Co(OH)₂, confirmed the surface composition changes with functionalization of ILs. In particular, the peak shift of O 1s from 529.66 eV of Co(OH)₂ to 530.14 eV of IL-Co(OH)₂ was attributed to the polarization via hydrogen bonding between the ILs and Co(OH)₂, which is consistent with the FT-IR results. These results elucidate that the hydrogen bond- co - π - π stacking interactions of ILs and Co(OH)₂ derived the formation of ultrathin nanosheet morphology and nanostructured hybrids.

To investigate the electrochemical energy storage behavior, cyclic voltammetry (CV) and galvanostatic

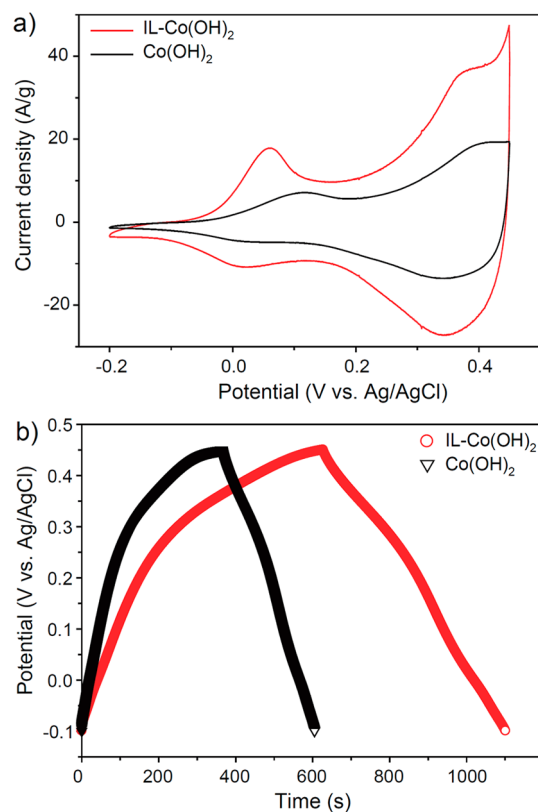


Figure 3. (a) CVs of Co(OH)₂ and IL-Co(OH)₂ electrodes at 50 mV/s in 3 M KOH solution and (b) galvanostatic charging/discharging behaviors of Co(OH)₂ and IL-Co(OH)₂ electrodes at a constant current density of 1 A/g in 3 M KOH solution.

charge/discharge measurements were performed on the Co(OH)₂ and IL-Co(OH)₂ electrodes as shown in Figure 3. The highly symmetrical CV curve (Figure 3a) of the IL-Co(OH)₂ electrode was observed with the forward and reverse sweeps, where two prominent redox peaks indicate the redox couple of Co(OH)₂/CoO₂.¹⁸ This showed a good pseudocapacitive response from the IL-Co(OH)₂ nanostructure. In particular, the introduction of ILs into the Co(OH)₂ structure led to a higher peak current, which is responsible for a higher charge capacity, compared to the bare Co(OH)₂. Figure 3b presents representative voltage–time profiles for the charging and discharging of the Co(OH)₂ and IL-Co(OH)₂ electrodes at a current density of 1 A/g. One can observe the pseudocapacitive characteristics of two electrodes, which is consistent with the redox peaks in the CV curves. The specific capacitance (C_s in F/g) was evaluated from the discharge curve as seen in eq 1:⁴

$$C_s = I/[m(\Delta V/\Delta t)] \quad (1)$$

where I is the applied constant current density, ΔV is the potential window, Δt is the discharge time, and m is the mass of the electrode. The specific capacitance of the IL-Co(OH)₂ electrode was calculated to be 859 F/g, which is 2-fold higher than that of the Co(OH)₂ electrode (418 F/g). It is evident from the CV and charging/discharging curves that the increase of the specific

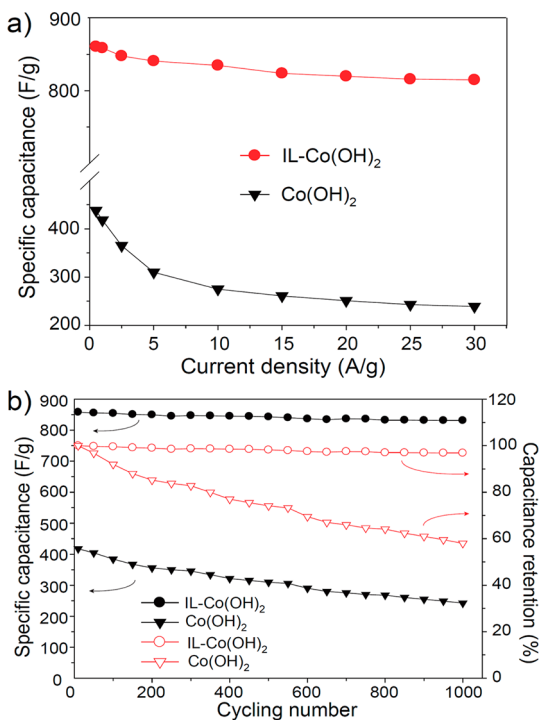


Figure 4. (a) Specific capacitances of the Co(OH)₂ and IL-Co(OH)₂ electrodes in the range of current density from 0.5 to 30 A/g. (b) Variation of specific capacitance and capacitance retention with 1000 cycling number for the Co(OH)₂ and IL-Co(OH)₂ electrodes at applied constant current density of 1 A/g.

capacitance value for hybrid materials compared with the bare Co(OH)₂ could be attributed to the effects of ILs on the enhancement of the redox reaction. When only Co(OH)₂ weight is counted (Supporting Information, Figure S3), the specific capacitance becomes approximately 895 F/g at a current density of 1 A/g. Although this value is lower than the theoretical value of 3460 F/g for Co(OH)₂,¹⁰ this is higher than those of other reported Co(OH)₂ materials, including urchin-like mesoporous Co(OH)₂¹⁸ and nanowire Co(OH)₂.¹³

The rate capability and cycle stability results as shown in Figure 4a and 4b highlight the merits of ILs in the high performance of IL-Co(OH)₂ hybrid electrodes. Figure 4a shows specific capacitance changes of Co(OH)₂ and IL-Co(OH)₂ electrodes with various current densities. As the current density increases from 0.5 to 30 A/g, the specific capacitance of the Co(OH)₂ electrode falls to a value of 239 F/g, retaining ~55% of its initial value. This poor rate capability of the Co(OH)₂ electrode can be attributed to the limitation of the ion diffusion at high-current density stemming from the time constraints.¹³ In contrast, the IL-Co(OH)₂ hybrid maintained a specific capacitance as high as 815 F/g (~95% retention) under the applied harsh current density of 30 A/g. As shown in Figure 4b, the long-term stability of both Co(OH)₂ and IL-Co(OH)₂ electrodes was evaluated during the repeated charging/discharging through 1000 cycles at 1 A/g of the applied

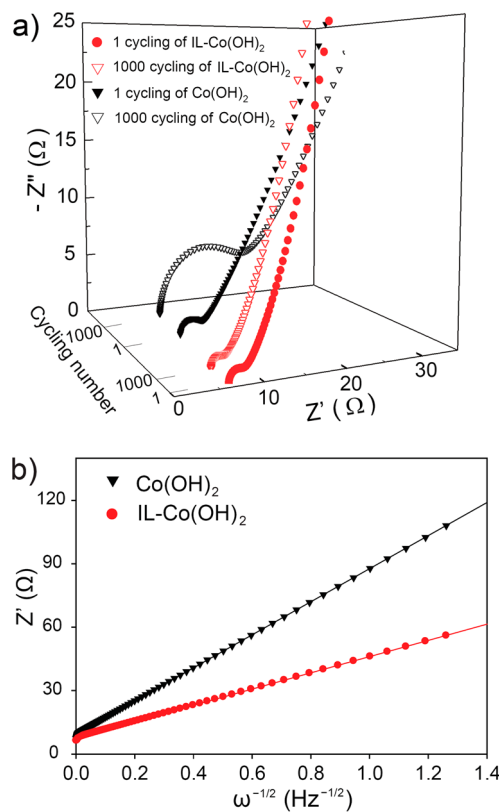
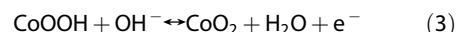


Figure 5. (a) Nyquist plots after 1 and 1000 charge-discharge cycles for the Co(OH)₂ and IL-Co(OH)₂ electrodes. (b) Plots of real part of impedance (Z') vs $\omega^{-1/2}$ for Co(OH)₂ and IL-Co(OH)₂ electrodes.

constant current density. After 1000 cycles, the Co(OH)₂ electrode showed a large capacitance loss, at 42% of the initial capacitance, whereas the capacitance of the IL-Co(OH)₂ electrode remained stable at a high level of ~96% retention up to 1000 cycles, indicating good cyclic stability of the hybrid electrode.

To gain deep insight into interfacial processes, we carried out AC impedance measurement on our samples. Faradaic redox reactions of the Co(OH)₂ electrode take place primarily on the electrode surface according to the following reactions:^{13,18}



For rapid and reversible redox reactions, three main points should be addressed: (i) ion and electron transport in electrode and electrolyte, (ii) electrochemical (redox) reactions at the electrode/electrolyte interface, and (iii) charge transfer at the interfaces. Figure 5a shows Nyquist plots of Co(OH)₂ and IL-Co(OH)₂ electrodes, representing the characteristic depressed semi-circle in the high- and medium-frequency regions and extended tail with respect to the real impedance in the low frequency region. The 1.53 Ω of charge-transfer resistance (R_{CT}) for the IL-Co(OH)₂ electrode, obtained from an equivalent circuit model,⁴³ was lower than that

of the Co(OH)_2 electrode (2.59Ω). This suggests that the functionalized IL- Co(OH)_2 improved interfacial characteristics and thus facilitated charge transfer. In particular, after 1000 cycles of CV, the R_{CT} value of IL- Co(OH)_2 electrode increased slightly from 1.53 to 1.55Ω , but the R_{CT} value of the Co(OH)_2 electrode increased significantly from 2.59 to 10.42Ω . It is worth noting that ILs on the Co(OH)_2 surface released the mechanical and structural stress by means of a buffering effect similar to the polymer electrolyte binder,⁴⁴ and thereby stabilized the electrochemical behavior during long cycling charge/discharge processes. In the low-frequency region, the IL- Co(OH)_2 electrode showed a more vertical Warburg slope (the straight line in the low frequency region) than the Co(OH)_2 electrode, indicating the enhanced fast ion movement on the IL- Co(OH)_2 electrode. In more detail, the real (Z') or imaginary (Z'') part was fitted following the angular frequency ($\omega^{-1/2}$) to determine the Warburg coefficient (σ), as shown in Figure 5b. From the plotting slope, the diffusion coefficient (D_{OH}) of electrolyte ions at the interfacial region can be calculated as follows: $1.06 \times 10^{-11} \text{ cm}^2/\text{s}$ for IL- Co(OH)_2 and $2.55 \times 10^{-12} \text{ cm}^2/\text{s}$ for Co(OH)_2 . The higher value of IL- Co(OH)_2 must be associated with fast and efficient ion pathways derived from a large surface area of mesopore structure and intrinsic properties of the highly ionic conductive ILs. Details on the ion diffusion calculation are given in the Supporting Information.

To understand the effect of IL on the redox reaction of Co(OH)_2 at the molecular level, we performed DFT calculations of a [Bmim][BF₄] molecule on the Co(OH)_2 surface. Details on the DFT calculations and results are given in Supporting Information (Figure S4–S9). The optimized structures of free [Bmim][BF₄] and [Bmim][BF₄] on the Co(OH)_2 surface are shown in Figure 6 panels a and b, respectively. The ionic binding between [Bmim] and [BF₄] is very strong with a binding energy of 4.28 eV , whereas the [Bmim][BF₄] molecule adsorbs moderately on the Co(OH)_2 surface with an adsorption energy of 0.62 eV . We examined the effect of the adsorbed [Bmim][BF₄] molecule on the desorption of surface hydrogen atoms of Co(OH)_2 . In Figure 6b, A, B, C, and D represent the surface hydrogen atoms beneath the [Bmim] cation or [BF₄] anion. We found that the [Bmim] cation facilitates the hydrogen desorption and the [BF₄] anion suppresses it: The hydrogen desorption energies are smaller (2.36, 2.65, and 2.54 eV for A, B, and C, respectively) and larger (2.87 eV for D) than the hydrogen desorption energy of 2.72 eV for a bare Co(OH)_2 surface (Supporting Information, Figure S9). Our results also imply that, when hydrogen atoms adsorb on the Co(OH)_2 surface without the topmost hydrogen atoms, the [Bmim] cation and [BF₄] anion exchange their roles as suppressor and facilitator for the hydrogen adsorption. Thus, IL plays a

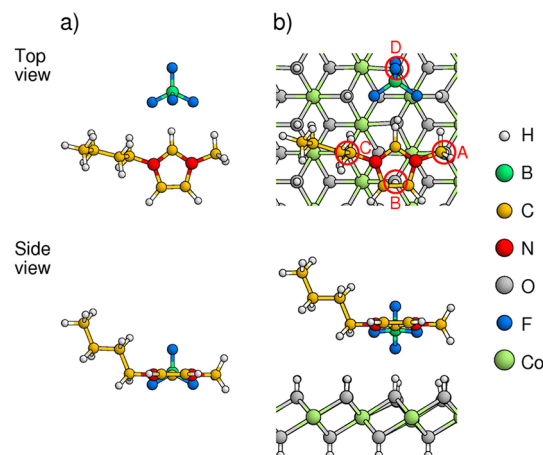


Figure 6. Optimized structures of (a) free [Bmim][BF₄] and (b) [Bmim][BF₄] on the Co(OH)_2 surface. A, B, C, and D represent the surface hydrogen atoms beneath the [Bmim] cation or [BF₄] anion.

key role by allowing easier hydrogen desorption/adsorption, that is, more favorable redox reactions, on the Co(OH)_2 surface.

It has been demonstrated that the creation of the IL- Co(OH)_2 hybrid can generate a rapid and reversible redox reaction through designing morphological and chemical structures, giving rise to good cycle performance and rate capability. IL-assisted synthesis offered the opportunity for a desirable morphology of the porous nanostructured networks of Co(OH)_2 with a large surface area and mesopore structure because of the template and cosolvent roles of ILs, as demonstrated by FT-IR and BET analyses. This entirely exposed nanohybrid surface enabled easy-access ion transfer, thereby leading to efficient redox reactions. The wetting behavior of ILs is also beneficial in the rapid surface adsorption of electrolyte ions. More importantly, ILs self-assembled on Co(OH)_2 by means of the hydrogen bond- $\text{co-}\pi-\pi$ stacking interaction serve as fast ion migration pathways, while continuously helping the adsorption/desorption process of hydrogen atoms. Compared with the bare Co(OH)_2 , a relatively smaller charge-transfer and higher electrolyte ion diffusion coefficient of IL- Co(OH)_2 demonstrated that the IL functionalities on Co(OH)_2 facilitated the interfacial processes and reduced ion diffusion length. Accordingly, the high-rate charging/discharging process of IL- Co(OH)_2 must be attributed to the enhanced electrochemical kinetics. Besides the aforementioned key advantages for this unique hybrid structure, its mechanical and structural stabilities are other attractive features. The high level of capacitance retention, at $\sim 95\%$, and the subtle change in Nyquist plots over 1000 cycles demonstrate the role of ILs as a protecting layer that can maintain the structural integrity of Co(OH)_2 and avoid the side reaction of oxygen evolution and reaggregation of Co(OH)_2 .

CONCLUSION

We reported the development of the nanoscale IL-Co(OH)₂ hybrid material showing rapid and reversible redox-based supercapacitive performance using the bottom-up self-assembly method. This synthetic method not only provided an extremely large BET surface area and mesoporous structure, but also altered surface chemistry. The electrochemical results presented here demonstrated the benefits of both the controlled morphology and the surface properties of nano-hybrids for rapid and efficient redox pseudocapacitance,

leading to a high specific capacitance, good rate capability, and remarkable cycling stability. In particular, AC impedance data and DFT calculations were comprehensively investigated to elucidate the critical role of ILs on the redox reaction; ILs allow for faster ion diffusion and easier hydrogen desorption/adsorption processes on the Co(OH)₂. The nanoscale design strategy demonstrated here can be generally applied in the synthesis of IL-based hybrids with other transition metal oxides or hydroxides for the development of energy storage devices, thereby allowing efficient electrochemical reactions.

EXPERIMENTAL SECTION

Chemicals. 1-Butyl-3-methylimidazolium tetrafluoroborate ([Bmim][BF₄]), high purity 99.9%, as the ionic liquid, was purchased from C-tri. Cobalt(II) chloride hexahydrate (CoCl₂·6H₂O, ACS reagent) was purchased from Aldrich. 1-Propanol and ammonium hydroxide (NH₄OH, 28 wt % in water) were obtained from Junsei. All reagents were used without further purification.

Synthesis of IL-Co(OH)₂ Nanohybrids. IL-Co(OH)₂ nanohybrids were prepared by the following experimental steps. CoCl₂·6H₂O (1.67 g) and 0.74 g of [Bmim][BF₄] were dissolved in 4 mL of a 3:1 mixture of 1-propanol and deionized (DI) water. The reaction solution was then stirred for 30 min at room temperature (RT). The 28 wt % NH₄OH was added dropwise into the above solution with continuous stirring until the pH of the solution reached 9. After aging at 80 °C for 12 h, the resultants were separated by filtration and rinsed several times with DI water and anhydrous ethanol, and finally air-dried at RT. As a negative control sample, Co(OH)₂ without [Bmim][BF₄] was prepared by the same explored procedure for IL-Co(OH)₂.

Preparation of the IL-Co(OH)₂ Electrode. The electrochemical properties of IL-Co(OH)₂ hybrids for pseudocapacitors were investigated by employing a conventional three-electrode electrochemical cell with an IL-Co(OH)₂ hybrid-based working electrode, a KCl-Ag/AgCl of reference electrode, and a platinum wire counter electrode. The electrolyte was 3 M KOH solution. The working electrode was fabricated using previously reported methods,¹⁸ pressing (*ca.* 10⁷ Pa) mixtures of 7.5 mg of as-prepared samples, 1.5 mg of acetylene black, and 1 mg of polytetrafluoroethylene (PTFE) binder onto a nickel foam (1 × 1 cm²) current collector. Before the performance measurements of the electrodes, as-obtained electrodes were dried and stored at 100 °C under vacuum.

Characterization. TEM images were collected using energy-filtering TEM (EM912Ω, Carl Zeiss) operating at 120 kV. High-resolution TEM images were obtained using field-emission TEM (JEM2100F, JEOL Ltd.) operating at 200 kV. XRD data were obtained on a Rigaku D/max IIIC (3 kW) with a θ/θ goniometer equipped with a CuKα radiation generator. N₂ adsorption/desorption was determined by BET measurements using an ASAP-2010 surface area analyzer. The BET method was used to calculate the specific surface area of samples. The pore size distributions were induced by the Barrett–Joyner–Halenda (BJH) model. The diffraction angle of the diffractograms was in the range of 2θ = 10°–80°. FT-IR spectra were collected on a JASCO FT-IR 470 plus. Each spectrum was recorded from 4000 to 400 cm⁻¹ using 12 scans at a resolution of 4 cm⁻¹. XPS data were obtained using a Thermo MultiLab 2000 system. Al Mg α X-ray source at 200 W was used with pass energy of 20 eV and 45° takeoff angle under 10⁻⁷ Torr vacuum analysis chamber. CV was performed with a CHI 760D electrochemical workstation (CH Instruments). Galvanostatic charge/discharge measurements were carried out using a Solartron 1287A. The electrochemical impedance spectroscopy measurements were performed over a frequency range from 10⁵ to 10⁻¹ Hz at the amplitude of the sinusoidal voltage of 10 mV using a Solartron 1260 impedance/gain-phase analyzer. A life cycling test was

performed using galvanostatic charge/discharge measurements at 1 A/g of current density up to 1000 cycles. All of the electrochemical measurements were performed at RT, and as-obtained data was within error range of ±1%. For a reference sample, a Co(OH)₂ electrode was prepared by the same protocol, which described the IL-Co(OH)₂ electrode.

Conflict of Interest: The authors declare no competing financial interest.

Acknowledgment. We acknowledge the financial support by the National Research Foundation of Korea Grant funded by the Korean Government (MEST, NRF-2010-C1AAA001-0029018) and by KBSI grant F32607. The work was also supported by the WCU program through the KOSEF under the MEST (grant number: R31-2008-000-10071-0).

Supporting Information Available: TEM images and BET of Co(OH)₂; TGA data of IL, Co(OH)₂, and IL-Co(OH)₂; detailed calculations of ion diffusion; computational details of DFT calculations; table for textural properties of Co(OH)₂ and IL-Co(OH)₂. This material is available free of charge via the Internet at <http://pubs.acs.org>.

REFERENCES AND NOTES

- Hall, P. J.; Mirzaeian, M.; Fletcher, S. I.; Sillars, F. B.; Rennie, A. J. R.; Shitta-Bey, G. O.; Wilson, G.; Cruden, A.; Carter, R. Energy Storage in Electrochemical Capacitors: Designing Functional Materials to Improve Performance. *Energy Environ. Sci.* **2010**, *3*, 1238–1251.
- Liu, C.; Li, F.; Ma, L.-P.; Cheng, H.-M. Advanced Materials for Energy Storage. *Adv. Mater.* **2010**, *22*, E28–E62.
- Zhang, L. L.; Zhao, X. S. Carbon-Based Materials as Supercapacitor Electrodes. *Chem. Soc. Rev.* **2009**, *38*, 2520–2531.
- Zhao, X.; Sánchez, B. M.; Dobson, P. J.; Grant, P. S. The Role of Nanomaterials in Redox-based Supercapacitors for Next Generation Energy Storage Devices. *Nanoscale* **2011**, *3*, 839–855.
- Wei, W.; Cui, X.; Chen, W.; Ivey, D. G. Manganese Oxide-Based Materials as Electrochemical Supercapacitor Electrodes. *Chem. Soc. Rev.* **2011**, *40*, 1697–1721.
- Lang, X.; Hirata, A.; Fujita, T.; Chen, M. Nanoporous Metal/Oxide Hybrid Electrodes for Electrochemical Supercapacitors. *Nat. Nanotechnol.* **2011**, *6*, 232–236.
- Brezesinski, T.; Wang, J.; Tolbert, S. H.; Dunn, B. Ordered Mesoporous α-MoO₃ with Iso-Oriented Nanocrystalline Walls for Thin-Film Pseudocapacitors. *Nat. Mater.* **2010**, *9*, 146–151.
- Ma, R.; Sasaki, T. Nanosheets of Oxides and Hydroxides: Ultimate 2D Charge-Bearing Functional Crystallites. *Adv. Mater.* **2010**, *22*, 5082–504.
- Guan, C.; Liu, J.; Cheng, C.; Li, H.; Li, X.; Zhou, W.; Zhang, H.; Fan, H. J. Hybrid Structure of Cobalt Monoxide Nanowire @ Nickel Hydroxide Nitrate Nanoflake Aligned on Nickel Foam for High-Rate Supercapacitor. *Energy Environ. Sci.* **2011**, *4*, 4496–4499.

10. Cao, L.; Xu, F.; Liang, Y.-Y.; Li, H.-L. Preparation of the Novel Nanocomposite Co(OH)₂/Ultra-Stable Y Zeolite and Its Application as a Supercapacitor with High Energy Density. *Adv. Mater.* **2004**, *16*, 1853–1857.
11. Wang, H.; Casalongue, H. S.; Liang, Y.; Dai, H. Ni(OH)₂ Nanoplates Grown on Graphene as Advanced Electrochemical Pseudocapacitor Materials. *J. Am. Chem. Soc.* **2010**, *132*, 7472–7477.
12. Chen, S.; Zhu, J.; Wang, X. One-Step Synthesis of Graphene–Cobalt Hydroxide Nanocomposites and Their Electrochemical Properties. *J. Phys. Chem. C* **2010**, *114*, 11829–11834.
13. Jiang, J.; Liu, J.; Ding, R.; Zhu, J.; Li, Y.; Hu, A.; Li, X.; Huang, X. Large-Scale Uniform α -Co(OH)₂ Long Nanowire Arrays Grown on Graphite as Pseudocapacitor Electrodes. *ACS Appl. Mater. Interfaces* **2011**, *3*, 99–103.
14. Jiang, H.; Zhao, T.; Li, C.; Ma, J. Hierarchical Self-Assembly of Ultrathin Nickel Hydroxide Nanoflakes for High-Performance Supercapacitors. *J. Mater. Chem.* **2011**, *21*, 3818–3823.
15. Liu, J.; Cheng, C.; Zhou, W.; Li, H.; Fan, H. J. Ultrathin Nickel Hydroxidenitrate Nanoflakes Branched on Nanowire Arrays for High-Rate Pseudocapacitive Energy Storage. *Chem. Commun.* **2011**, *47*, 3436–3438.
16. Lu, Z.; Chang, Z.; Zhu, W.; Sun, X. Beta-Phased Ni(OH)₂ Nanowall Film with Reversible Capacitance Higher than Theoretical Faradic Capacitance. *Chem. Commun.* **2011**, *47*, 9651–9653.
17. Zhou, W.; Zhang, J.; Xue, T.; Zhao, D.; Li, H. Electrodeposition of Ordered Mesoporous Cobalt Hydroxide Film from Lyotropic Liquid Crystal Media for Electrochemical Capacitors. *J. Mater. Chem.* **2008**, *18*, 905–910.
18. Yuan, C.; Zhang, X.; Hou, L.; Shen, L.; Li, D.; Zhang, F.; Fan, C.; Li, J. Lysine-Assisted Hydrothermal Synthesis of Urchin-like Ordered Arrays of Mesoporous Co(OH)₂ Nanowires and Their Application in Electrochemical Capacitors. *J. Mater. Chem.* **2010**, *20*, 10809–10816.
19. Simon, P.; Gogotsi, Y. Materials for Electrochemical Capacitors. *Nat. Mater.* **2008**, *7*, 845–854.
20. Liu, R.; Duay, J.; Lee, S. B. Heterogeneous Nanostructured Electrode Materials for Electrochemical Energy Storage. *Chem. Commun.* **2011**, *47*, 1384–1404.
21. Maier, J. Nanoionics: Ion Transport and Electrochemical Storage in Confined Systems. *Nat. Mater.* **2005**, *4*, 805–815.
22. Hu, C.-C.; Chang, K.-H.; Lin, M.-C.; Wu, Y.-T. Design and Tailoring of the Nanotubular Arrayed Architecture of Hydrous RuO₂ for Next Generation Supercapacitors. *Nano Lett.* **2006**, *6*, 2690–2695.
23. Antonietti, M.; Kuang, D.; Smarsly, B.; Zhou, Y. Ionic Liquids for the Convenient Synthesis of Functional Nanoparticles and Other Inorganic Nanostructures. *Angew. Chem., Int. Ed.* **2004**, *43*, 4988–4992.
24. Park, H. S.; Choi, Y. S.; Jung, Y. M.; Hong, W. H. Intermolecular Interaction-Induced Hierarchical Transformation in 1D Nanohybrids: Analysis of Conformational Changes by 2D Correlation Spectroscopy. *J. Am. Chem. Soc.* **2008**, *130*, 845–852.
25. Park, H.; Yang, S. H.; Jun, Y.-S.; Hong, W. H.; Kang, J. K. Facile Route to Synthesize Large-Mesoporous γ -Alumina by Room Temperature Ionic Liquids. *Chem. Mater.* **2007**, *19*, 535–542.
26. Zhang, Y.; Shen, Y.; Yuan, J.; Han, D.; Wang, Z.; Zhang, Q.; Niu, L. Design and Synthesis of Multifunctional Materials Based on an Ionic-Liquid Backbone. *Angew. Chem., Int. Ed.* **2006**, *45*, 5867–5870.
27. Choi, D. S.; Kim, D. H.; Shin, U. S.; Deshmukh, R. R.; Lee, S.; Song, C. E. The Dramatic Acceleration Effect of Imidazolium Ionic Liquids on Electron Transfer Reactions. *Chem. Commun.* **2007**, 3467–3469.
28. Kim, T.; Lee, H.; Kim, J.; Suh, K. S. Synthesis of Phase Transferable Graphene Sheets Using Ionic Liquid Polymers. *ACS Nano* **2010**, *4*, 1612–1618.
29. Pringle, J. M.; Winther-Jensen, O.; Lynam, C.; Wallace, G. G.; Forsyth, M.; MacFarlane, D. R. One-Step Synthesis of Conducting Polymer-Noble Metal Nanoparticle Composites Using an Ionic Liquid. *Adv. Funct. Mater.* **2008**, *18*, 2031–2040.
30. Marcilla, R.; Curri, M. L.; Cozzoli, P. D.; Martínez, M. T.; Loinaz, I.; Grande, H.; Pomposo, J. A.; Mecerreyres, D. Nano-Objects on a Round Trip from Water to Organics in a Polymeric Ionic Liquid Vehicle. *Small* **2006**, *2*, 507–512.
31. Cai, R.; Sun, M.; Chen, Z.; Munoz, R.; O'Neill, C.; Beving, D. E.; Yan, Y. Ionothermal Synthesis of Oriented Zeolite AEL Films and Their Application as Corrosion-Resistant Coatings. *Angew. Chem., Int. Ed.* **2008**, *47*, 525–528.
32. Armand, M.; Endres, F.; MacFarlane, D. R.; Ohno, H.; Scrosati, B. Ionic-Liquid Materials for the Electrochemical Challenges of the Future. *Nat. Mater.* **2009**, *8*, 621–629.
33. Sillars, F. B.; Fletcher, S. I.; Mirzaei, M.; Hall, P. J. Effect of Activated Carbon Xerogel Pore Size on the Capacitance Performance of Ionic Liquid Electrolytes. *Energy Environ. Sci.* **2011**, *4*, 695–706.
34. Wishart, J. F. Energy Applications of Ionic Liquids. *Energy Environ. Sci.* **2009**, *2*, 956–961.
35. Moganty, S. S.; Jayaprakash, N.; Nugent, J. L.; Shen, J.; Archer, L. A. Ionic-Liquid-Tethered Nanoparticles: Hybrid Electrolytes. *Angew. Chem., Int. Ed.* **2010**, *49*, 9158–9161.
36. Brunauer, S.; Emmett, P. H.; Teller, E. Adsorption of Gases in Multimolecular Layers. *J. Am. Chem. Soc.* **1938**, *60*, 309–319.
37. Chakoumakos, B. C.; Loong, C.-K.; Schultz, A. J. Low-Temperature Structure and Dynamics of Brucite. *J. Phys. Chem. B* **1997**, *101*, 9458–9462.
38. Liu, Z.; Ma, R.; Osada, M.; Takada, K.; Sasaki, T. Selective and Controlled Synthesis of α - and β -Cobalt Hydroxide in Highly Developed Hexagonal Platelets. *J. Am. Chem. Soc.* **2005**, *127*, 13869–13874.
39. Sing, K. S. W.; Everett, D. H.; Haul, R. A. W.; Moscou, L.; Pierotti, R. A.; Rouquérol, J.; Siemieniewska, T. Reporting Physisorption Data for Gas/Solid Systems with Special Reference to the Determination of Surface Area and Porosity. *Pure Appl. Chem.* **1985**, *57*, 603–619.
40. Zhou, Y.; Schattka, J. H.; Antonietti, M. Room-Temperature Ionic Liquids as Template to Monolithic Mesoporous Silica with Wormlike Pores via a Sol–Gel Nanocasting Technique. *Nano Lett.* **2004**, *4*, 477–481.
41. Lian, J.; Duan, X.; Ma, J.; Peng, P.; Kim, T.; Zheng, W. Hematite (α -Fe₂O₃) with Various Morphologies: Ionic Liquid-Assisted Synthesis, Formation Mechanism, and Properties. *ACS Nano* **2009**, *3*, 3749–3761.
42. Martineze, C. R.; Iverson, B. L. Rethinking the term “pi-stacking”. *Chem. Sci.* **2012**, *3*, 2191–2201.
43. Li, X.; Rong, J.; Wei, B. Electrochemical Behavior of Single-Walled Carbon Nanotube Supercapacitors under Compressive Stress. *ACS Nano* **2010**, *4*, 6039–6049.
44. Liu, W.-R.; Yang, M.-H.; Wu, H.-C.; Chiao, S. M.; Wu, N.-L. Enhanced Cycle Life of Si Anode for Li-Ion Batteries by Using Modified Elastomeric Binder. *Electrochim. Solid-State Lett.* **2005**, *8*, A100–A103.